Dynamic behavior of non-linear planetary gear model in non-stationary conditions

Ahmed Hammami[1], Ayoub Mbarek[1,2] , Alfonso Fernández[2], Fakher Chaari[1] , Fernando Viadero[2], Mohamed Haddar[1]

[1] Mechanics, Modelling and Production Laboratory, National School of Engineers Sfax, Tunisia

Ahmed.hammami2109@gmail.com

[2] Department of Structural and Mechanical Engineering, University of Cantabria, Spain

Abstract:

The nonlinear effects in gearboxes are a key concern to describe accurately their dynamic behavior. This task is difficult for complex gear systems such as planetary gearboxes. The main aim of this work is provide responses to overcome this difficulty especially in non-stationary operating regimes by investigating a back-to-back planetary gearbox in steady conditions and in run up regime.

The nonlinear Hertzian contact of teeth pair is modeled in stationary and non-stationary run-up regime. Then it is incorporated to a torsional model of the planetary gearbox through the different mesh stiffness functions.

In addition, motor torque and external load variation are taken into account. The nonlinear equations of motion of the back-to-back planetary gearbox are computed through the Newmark-β algorithm combined with the method of Newton-Raphson. An experimental validation of the proposed numerical model is done through a test bench for both stationary and run-up regimes. The vibration characteristics are extracted and correlated to speed and torque. Time frequency analysis is implemented to characterize the transient regime during run-up.

Keys words: planetary gear**,** non-linearity**,** run up regime, stationary condition

Nomenclature	
α_m	The operating pressure angle
F	The external applied force
G	Shear modulus
s_h	Shear factor
I_i	The inertia
A_i	Area moment
S_i	The cross section of tooth
ν	The Poisson ratio
E	Young's modulus
W	Tooth width
S_b	The slip at breakdown
T_b	the torque at breakdown,
a_1 and b_1	Motor constant properties
f_s	Sun rotational frequency
Z_s	Sun teeth number
Z_r	Ring teeth number
s	The proportional drop in the speed
Notation	
HS	Hertzian Stiffness
BS	Bending Stiffness
FFS	Fillet Foundation Stiffness
TE	Transmission Error
FEM	Finite Element Method

1-Introduction:

Planetary gears are operated in several fields such as wind turbine and hybrid automotive where the performance of the whole system particularly depends on the split unit [1-3]. Many researchers proposed numerical models of planetary gears in order to ameliorate its dynamic behavior [4-13] and to have a better understanding of the vibratory signature, allowing the development of more efficient fault detection and diagnostic techniques [14-18].

The variable speed and load are the main non-stationary conditions in which planetary gears are usually running. These conditions externally excite the planetary gearbox [19]. For this, machinery dynamic behaviour for varying speed conditions is a very attractive research topic. Chaari et al., [20] studied planetary gearbox dynamic behaviour running under variable loading which induce variability in the motor speed. Obtained results are presented by using the STFT (Short Time Fourier Transform). Zimroz et al. [21] proposed an automatic time-frequency segmentation algorithm to highlight effects of load and speed varying conditions on planetary gearbox dynamics. Vicuña and Chaari [22] carried out running experiments of planetary gearbox under sinusoidal variable load to which the input speed is sensitive. They correlated these measurements with numerical results obtained from a dynamic model in which the gear mesh stiffness depends on the input speed. Lopatinskaia et al., [23, 24] proposed to analyze the vibration signal in the angle domain. Meltzer and Ivanov [25, 26] processed signals of a three-stage planetary gearbox test bench through time quefrency techniques to detect tooth defects during start up and run down. Zimroz et al., [27] investigated the variable input wind power effect on gearbox vibrations of a wind turbine. They presented the STFT of the gearbox to show the frequency modulations. Viadero et al. [28] numerically studied the behavior of an offshore wind turbine gearbox which is subject to fast run-up and emergency run-down. During start up, the gear mesh stiffness between gears is modeled with sinusoidal functions where meshing period decreases in time. Hammami et al., [29-30] studied the planetary gearbox dynamic behavior during start up and stop regimes [29] and under variable speed [30]. The gear mesh stiffness sun-planets and planets-ring are modeled with rectangular waves respecting the meshing phase between planets. In these works [29, 30], the meshing period is decreasing when speed is increasing.

These cited works on time varying speed gearbox used linear gear mesh stiffness to model the teeth gear contacts which are the main internal excitations.

In general, the teeth contact are modeled by the gear mesh stiffness functions which are computed by considering only the teeth HS or considering both HS, BS of tooth and FFS.

In many researchers' works, the nonlinear contact between teeth is taken into account. In fact, Zhou et al., [31] investigated the nonlinear dynamic effects of backlash, friction and load of gear-rotor-bearing system through a lateral-torsional model and they highlighted the quasi-periodic behavior due to these effects. The sixteen d-o-f responses are computed by using Runge-Kutta algorithm. In addition, Chen et al., [32] computed the non-linear vibration response of a face gearbox which is excited by the mesh stiffness, backlash and stiffness of supports. They also used Runge-Kutta algorithm to compute the non-linear equation of motion. Fernandez et al., [33] used the hertzian contact theory and the FEM method to compute the load TE and the mesh stiffness function of spur gear.

The modeling of the non-linear planetary gear system is extensively studied nowadays. Guo et al. [34] examined the stability and the nonlinear behavior of wind turbine planetary gearbox by using the FEM and lumped parameters methods in which the corresponding dynamic response is computed with the help of the extended harmonic balance method. They correlated the analytical and the numerical results to those obtained experimentally. Zhao and Ji [35] have concluded that the external excitation and the mesh stiffness are the main significant factors which have influence on the nonlinear dynamic behavior of wind turbine gearbox which is computed by the numerical integration method. Guo and Parker [36] showed that the non-linearity caused by bearing clearance can decrease the resonances in helicopter gear sets. Also, the dynamic behavior of spur planetary gear in different backlashes is investigated by Liu et al., [37] through a lumped-parameter model which considered the nonlinearity introduced by the gravity effect and bearing oil film. They used Newmark integration to calculate the dynamic responses. Nevertheless, dynamic models of planetary gears should include a non-linear mesh stiffness function and gear contact loss nonlinearity [38-41]. The influence of nonlinear jumps and the chaotic motions on dynamic behavior of planetary gearbox is studied by Ambarisha and Parker [42] who correlated their analytical results with FEM results.

Most nonlinear cited models are exploited under stationary operation where the speed is constant and used Runge-Kutta method or Newmark integration to compute the nonlinear dynamic response. Although, Bouchaala et al., [43] investigated the effect of nonlinear Hertzian gear contact on the vibration behavior of one-stage spur gearbox in acyclism regime, their work presents only a theoretical contribution without any experimental validation.

In the concrete conditions, the contact between teeth in planetary gearbox needs to be considered in the dynamic models especially when the gearbox is running in the non-stationary conditions. Thus, the non-linear hertzian contact between teeth is a basic condition to refine the gear dynamic analysis and to allow a better diagnosis when the driven speed or the applied

loads are variable. The aim of this work is to check the influence of considering non-linear (HS) between mating teeth on the vibration behavior of planetary gearbox. A corresponding nonlinear model is developed to study this effect. Using Newmark-Newton Raphson integration method, the dynamic response is computed under two regimes: stationary conditions and variable speed conditions and the example of run-up regime will be studied in this case. Numerical results are compared to those obtained from experience through a planetary gearbox test bench.

2- Test bench description:

The test bench is configured in a two-spur identical planetary gear with 3 planets (Fig. 1).
The two gear sets are linked in a back-to-back configuration through a rigid shaft and a hollow shaft respectively called sun's shaft and carrier shafts. This special configuration allows minimizing costs and improving energy efficiency. The test gear set is the main planetary gear set in which output power from test carrier is reintroduced to the input test sun with the help of the reaction gear set [47]. Moreover, an external torque can mechanically be applied to the reaction ring gear by adding masses on the arm.

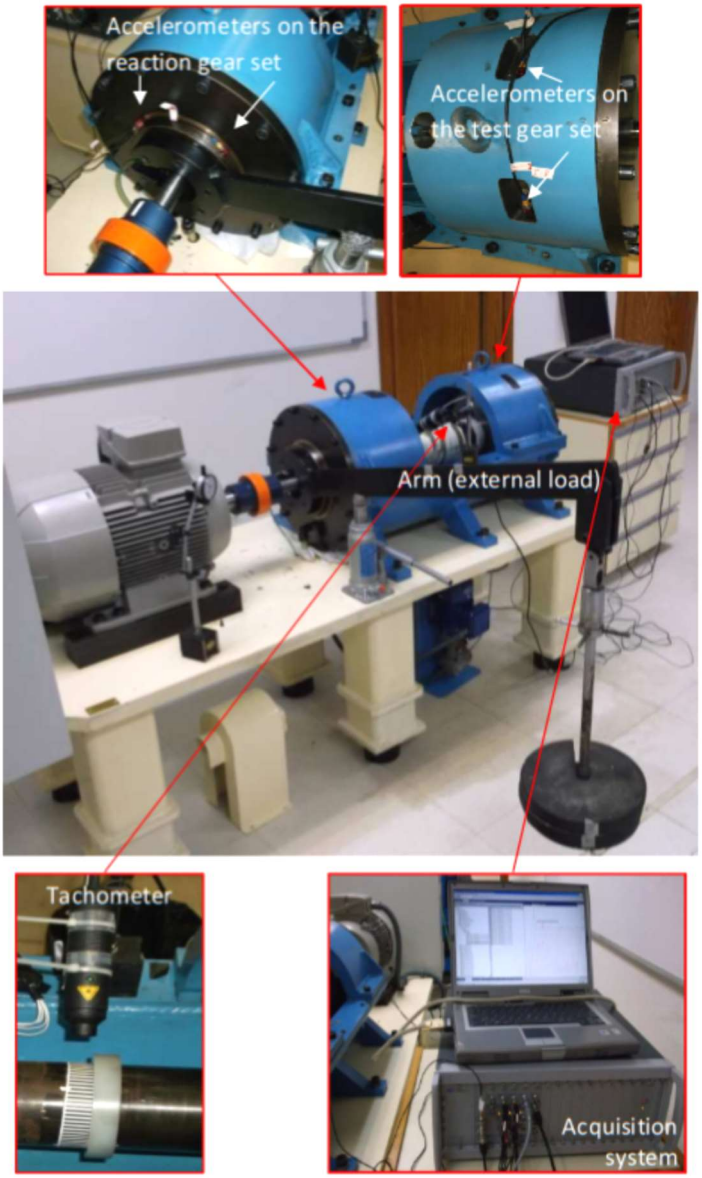

(a)

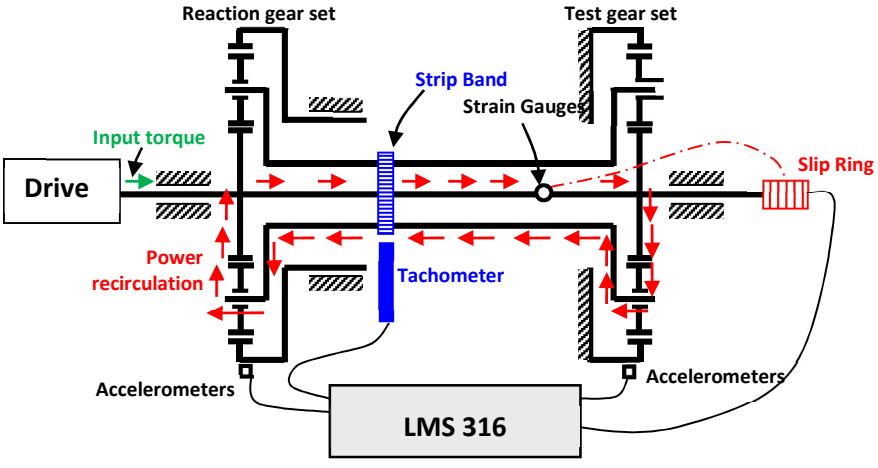

(b)

Fig. 1 (a) Planetary gearbox test bench (b) instrumentation layout

The driving electric motor is connected to the reaction gear with a rigid shaft and it is controlled by a variable frequency converter which is configured with "STARTER" software. Four accelerometers are fixed on each ring. In addition, an optic tachometer recorded the instantaneous angular velocity of the hollow shaft. The signals coming from accelerometers and tachometer are acquired by an acquisition LMS SCADAS 316 system.

Additional key parameters of this test bench are illustrated in table 1. Further details about the test bench can be found in [44-46].

Table 1 Basic dimensions of planetary gear

	Ring	Planet (3)	Sun	Carrier
Number of teeth	65	24	16	-
Mass (Kg)	28.1	1.225	0.485	3.643
Moment of inertia (Kgm^2)	$697767 \cdot 10^{-6}$	$2045 \cdot 10^{-6}$	$356 \cdot 10^{-6}$	$21502 \cdot 10^{-6}$
Base diameters (m)	0.2494	0.0921	0.0614	0.1728
Tip diameters (m)	0.2579	0.1006	0.0699	0.1813
Module (mm)		4.23		
Pressure angle (rad)		0.4621		

3-Modelling of gear mesh-stiffness:

The gear mesh stiffness of both sun-planets and ring-planets are modeled by putting in series the different stiffness (figure 2): BS "K_b", the FFS "K_f" and the HS "K_h".

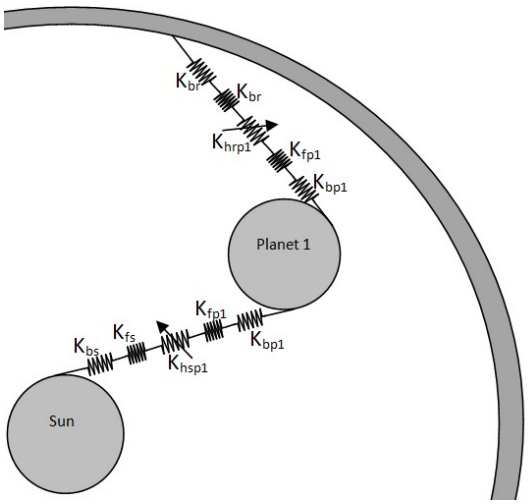

Fig. 2 Nonlinear mesh stiffness sun-planet 1 and ring-planet 1

$$K_{jik} = \frac{1}{\frac{1}{K_{bipk}}+\frac{1}{K_{fpk}}+\frac{1}{K_{bi}}+\frac{1}{K_{fi}}+\frac{1}{K_{hi}}} \quad (1)$$

Where i=r,t (r for the reaction gear set and t for the test gear set), i=s, r (s for the sun gear and r for the ring gear) and k=1..3 (planet order). The variable mesh stiffness $K_i(t)$ can be quantified based on the procedure given by Velex and Flamand [40]. The mesh period is defined by:

$$T_s = \frac{Z_s Z_r}{(Z_s+Z_s)} \frac{N}{60} \quad (2)$$

1-3-Bending deflection

Based on the results obtained by Cornell [48], the bending deflection δ_b is expressed as:

$$\delta_b = F\cos^2\alpha_m \sum_{i=1}^{n} e_i \left\{ \frac{d_i - e_i d_i + \frac{e_i^2}{3}}{E\prime \overline{I_i}} + \frac{1}{s_h G \overline{A_i}} + \frac{\tan^2\alpha_m}{E\prime \overline{A_i}} \right\} \quad (3)$$

e_i is the considered segment width of the tooth which is supposed segmented uniform cantilever beam. d_i is the distance between the considered segment and the cross point between the tooth symmetric line and the line of action.

E′, I_i and A_i are defined as following :

$$E' = \frac{E(1-\nu)}{(1+\nu)(1-2\nu)} \quad (4)$$

$$\frac{1}{\overline{I_I}} = \frac{\frac{1}{I_i}+\frac{1}{I_{i+1}}}{2} \quad (5)$$

$$\frac{1}{\overline{A_i}} = \frac{\frac{1}{A_i}+\frac{1}{A_{i+1}}}{2} \quad (6)$$

The corresponding (BS) can be obtained by:

$$k_b = \frac{F}{\delta_B} \quad (7)$$

2-3-Fillet foundation deflection

It is modeled according to Muskhelishvili theory [49]:

$$\delta_f = \frac{F co^{\,2}\alpha_m}{WE} \left\{ L^* \left(\frac{u_f}{S_f}\right)^2 + M^* \left(\frac{u_f}{S_f}\right) + P^*(1 + Q^* tan^2\alpha_m) \right\} \quad (8)$$

Where S_f is the dedendum surface of the tooth and u_f is the distance between the dedendum circle and the crossing point between the tooth symmetric line and the line of action.

L*, M*, P*and Q* are polynomial functions defined by Sainsot et al. [50].

$$X_i^*(h_{fi}, \theta_f) = \frac{A_i}{\theta_f^2} + \frac{B_i}{h_{fi}^2} + \frac{C_i h_{fi}}{\theta_f} + \frac{D_i}{\theta_f} + E_i h_{fi} + F_i \quad (9)$$

$h_{fi} = r_f/r_{int}$, r_f and θ_f are respectively the radius of the dedendum circle and the dedendum angular pitch of the tooth.

The (FFS) can be deduced by:

$$K_f = \frac{F}{\delta_f} \tag{10}$$

3-3-Contact deflection

The following equation presents the Hertzian elastic deformation in the line contact derived by Harsha [51]:

$$\delta_h = \frac{4.05F_0^{0.925}}{10^5 l_{eff}^{0.85}} \tag{11}$$

Where l_{eff} is the length of contact between teeth. The deflection contact force is indicated by:

$$F_h = 56065.703 l_{eff}^{0.92} \delta_h^{1.08} \tag{12}$$

Thus, the non-linear deflection stiffness is given by:

$$K_h = \frac{F_h}{\delta_h} = 56065.703 l_{eff}^{0.92} \delta_h^{0.08} \tag{13}$$

4-Numerical model:

A torsional model corresponding to the test bench is developed [47] and it is shown in Fig.3.

This paper assumes that all planetary gears component has a rotational rigid motion.

The model consisted of two similar planetary gear sets called reaction gear and test gear respectively. The reaction ring is located near the motor, it is characterized as a free ring.

Two rigid shafts were used to link the inner parts (suns and carriers) and a rigid housing was used to link the external parts (ring). The sun reaction gear is connected to input shaft and the free ring is connected to a rigid arm and extorted by the external torque.

The mass and inertia of each components were denoted m_c, I_c, m_s, I_s, m_r, I_r, m_{p1}, I_{p1}, m_{p2}, I_{p2}, m_{p3}, I_{p3} for the carrier, the sun, the ring and the three planets respectively.

The planets were linked to the reaction ring by the ring planets mesh stiffness K_{rr1} K_{rr2} and K_{rr3} and to the reaction sun by the sun planets mesh stiffness K_{sr1}, K_{sr2} and K_{sr3} respectively. The same functions were used in the test gear. They are K_{rt1} K_{rt2} and K_{rt3}ring planets mesh stiffness and K_{st1}, K_{st2} and K_{st3} sun planets mesh stiffness.

The sun's shaft and the carrier's shaft are respectively modeled by a torsional stiffness k_{st} and k_{ct}.

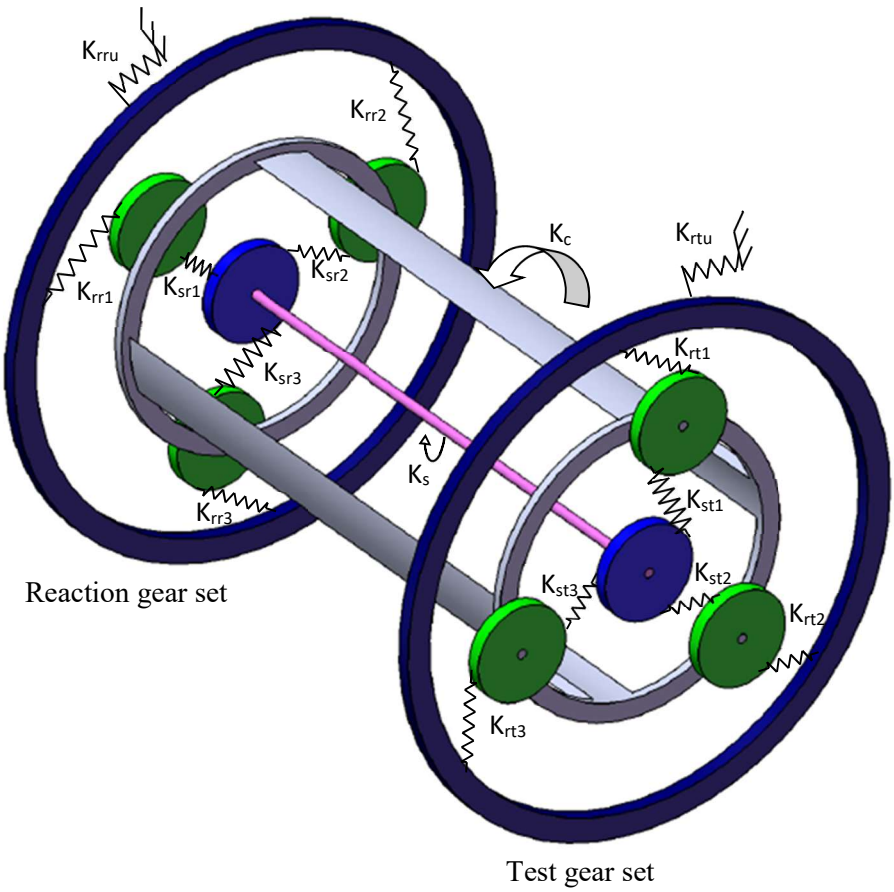

Fig. 3 Planetary gear torsional model

The corresponding equation of motion is:

$$M\ddot{q} + C\dot{q} + K_c q + F_{nl} = F_{ext}(t) \tag{14}$$

Only the rotational movements were considered.

$$q = \{\theta_{cr} \quad \theta_{rr} \quad \theta_{sr} \quad \theta_{p1r} \quad \theta_{p2r} \quad \theta_{p3r} \quad \theta_{ct} \quad \theta_{rt} \quad \theta_{st} \quad \theta_{p1t} \quad \theta_{p2t} \quad \theta_{p3t}\} \tag{15}$$

q is the d-o-f vector of the system, M denotes the mass matrix.

$$M = \begin{bmatrix} M_r & 0 \\ 0 & M_t \end{bmatrix} \tag{16}$$

$$M_i = diag\left(\frac{I_{ci}}{r_{ci}} + n.m_p \quad \frac{I_{ri}}{r_{ri}} \quad \frac{I_{si}}{r_{si}} \quad \frac{I_{p1i}}{r_{p1i}} \quad \frac{I_{p2i}}{r_{p2i}} \quad \frac{I_{p3i}}{r_{p3i}}\right) \text{ i=r,t} \tag{17}$$

$$K(t) = \begin{bmatrix} K_{mr} & 0 \\ 0 & K_{mt} \end{bmatrix} + K_c \tag{18}$$

$$K_{mr} =$$

$$\begin{bmatrix} \sum_{i=1}^{3}(K_{sri}(t)+K_{rri}(t)) & -\sum_{i=1}^{3}K_{rri}(t) & -\sum_{i=1}^{3}K_{rri}(t) & K_{rr1}(t)-K_{sr1}(t) & K_{rr2}(t)-K_{sr2}(t) & K_{rr3}(t)-K_{sr3}(t) \\ -\sum_{i=1}^{3}K_{rri}(t) & \sum_{i=1}^{3}K_{rri}(t) & 0 & -K_{rr1}(t) & -K_{rr2}(t) & -K_{rr3}(t) \\ -\sum_{i=1}^{3}K_{sri}(t) & 0 & \sum_{i=1}^{3}K_{sri}(t) & K_{sr1}(t) & K_{sr2}(t) & K_{sr3}(t) \\ K_{rr1}(t)-K_{sr1}(t) & -K_{rr1}(t) & K_{sr1}(t) & K_{sr1}(t)+K_{rr1}(t) & 0 & 0 \\ K_{rr2}(t)-K_{sr2}(t) & -K_{rr2}(t) & K_{sr2}(t) & 0 & K_{sr2}(t)+K_{rr2}(t) & 0 \\ K_{rr3}(t)-K_{sr3}(t) & -K_{rr3}(t) & K_{sr3}(t) & 0 & 0 & K_{sr3}(t)+K_{rr3}(t) \end{bmatrix} \quad (19)$$

$$K_{mt} =$$

$$\begin{bmatrix} \sum_{i=1}^{3}(K_{sti}(t)+K_{rti}(t)) & -\sum_{i=1}^{3}K_{rti}(t) & -\sum_{i=1}^{3}K_{rti}(t) & K_{rt1}(t)-K_{st1}(t) & K_{rt2}(t)-K_{st2}(t) & K_{rt3}(t)-K_{st3}(t) \\ -\sum_{i=1}^{3}K_{rti}(t) & \sum_{i=1}^{3}K_{rti}(t) & 0 & -K_{rt1}(t) & -K_{rt2}(t) & -K_{rt3}(t) \\ -\sum_{i=1}^{3}K_{sti}(t) & 0 & \sum_{i=1}^{3}K_{sti}(t) & K_{st1}(t) & K_{st2}(t) & K_{st3}(t) \\ K_{rt1}(t)-K_{st1}(t) & -K_{rt1}(t) & K_{st1}(t) & K_{st1}(t)+K_{rt1}(t) & 0 & 0 \\ K_{rt2}(t)-K_{st2}(t) & -K_{rt2}(t) & K_{st2}(t) & 0 & K_{st2}(t)+K_{rt2}(t) & 0 \\ K_{rt3}(t)-K_{st3}(t) & -K_{rt3}(t) & K_{st3}(t) & 0 & 0 & K_{st3}(t)+K_{rt3}(t) \end{bmatrix} \quad (20)$$

The damping matrix "C" is defined as:

$$C = \alpha M + \beta K \quad (21)$$

α and β are two constants.

The external torque vector F_{ext} is expressed as:

$$F_{ext} = \{0 \quad 0 \quad C_m(t) \quad 0 \quad 0 \quad 0 \quad 0 \quad 0 \quad C_r(t) \quad 0 \quad 0 \quad 0\} \quad (22)$$

The nonlinear force induced by the HS and expressed as following:

$$F_{nl} = \{X\}K_i(t)\{X\}^T\{q\} = \{X\}K_i(t)\delta \quad (23)$$

This force is defined as:

$$F_{nl} = \{F_{nl,r} \quad F_{nl,t}\}^T \quad (24)$$

$$F_{nl,j}(t) = \{0 \quad F_{rj}(t) \quad F_{sj}(t) \quad F_{p1j}(t) \quad F_{p2j}(t) \quad F_{p3j}(t)\}^T \quad (25)$$

$$F_{rj}(t) = -\sum_{i=1}^{n} K_{rij}(t)\delta_{ri}^{j}(t)\{r_{1i} \quad r_{2i} \quad r_{3i}\}^T \quad (26)$$

$$F_{sj}(t) = -\sum_{i=1}^{n} K_{sij}(t)\delta_{si}^{j}(t)\{s_{1i} \quad s_{2i} \quad s_{3i}\}^T \quad (27)$$

$$F_{ij}(t) = -K_{rij}(t)\delta^{j}_{ri}(t)\{r_{4i} \quad r_{5i} \quad r_{6i}\}^{T} - K_{sij}(t)\delta^{j}_{si}(t)\{s_{4i} \quad s_{5i} \quad s_{6i}\}^{T} \text{ , avec i=1..3} \qquad (28)$$

The tooth deflection components are highlighted in table 2.

Table 2 Tooth deflection components

Coefficients s_i	**Coefficients r_i**
$s_{1i}=s_{2i}=s_{3i}=-r_{br}$	$r_{1i}=r_{2i}=r_{3i}=-r_{bp}$
$s_{4i}=s_{5i}=s_{6i}=r_{bs}$	$r_{4i}=r_{5i}=r_{6i}=r_{bp}$

With:

$$\{X\} = \{r_{bcr} \quad r_{brr} \quad r_{bsr} \quad r_{bp1r} \quad r_{bp2r} \quad r_{bp3r} \quad r_{bct} \quad r_{brt} \quad r_{bst} \quad r_{bp1t} \quad r_{bp2t} \quad r_{bp3t}\}^{T} \qquad (29)$$

The TE "δ" is defined by Velex and Flamand [26]:

$$\delta^{r}_{ri} = r_{brr}\theta_{rr} + r_{bir}\theta_{ir} \qquad (30)$$

$$\delta^{t}_{ri} = r_{brt}\theta_{rt} + r_{bit}\theta_{it} \qquad (31)$$

$$\delta^{r}_{si} = r_{bsr}\theta_{sr} + r_{bir}\theta_{ir} \qquad (32)$$

$$\delta^{t}_{si} = r_{bst}\theta_{st} + r_{bit}\theta_{it} \qquad (33)$$

Characteristics of the mechanical transmissions are shown on table 3.

Table 3 Model parameters.

	Torsional Shaft Stiffness (Nm/rd)
Sun	$3.73 \cdot 10^{4}$
Carrier	$8.38 \cdot 10^{5}$
	Gear Mesh stiffness[N/m]
Sun-planets	$3.5.10^{8}$
Planets-ring	$4.5.10^{8}$

The equation of motion is computed using the classical Newton Raphson method coupled with the implicit Newmark algorithm.

Before applying the Newmark method, we need firstly to compute the initial value correspondent to $X_0, \dot{X}_0, \ddot{X}_0$.Then, the equation of motion (14) is transformed to an approximated version ($t= t_{n+1}$):

$$M\{\ddot{q}\}_{n+1} + C\{\dot{q}\}_{n+1} + K_c\{q\}_{n+1} + F_{nl}\{X\}_{n+1} = \{F_{ext}(t)\}_{n+1} \qquad (34)$$

Firstly, the initial displacement, velocity and acceleration are introduced:

$d_0 = q(0), v_0 = \dot{q}(0)$, $a_0 = \ddot{q}(0)$

$$\{X\}_{i+1} = \{X\}_i + \Delta t\{\dot{X}\}_i + b\Delta t^2\left[\left(\frac{1}{2b} - 1\right)\{\ddot{X}\}_i + \{\ddot{X}\}_{i+1}\right] \quad (35)$$

$$\{\dot{X}\}_{i+1} = \{\dot{X}\}_i + \Delta t(1-a)\{\ddot{X}\}_i + a\Delta t\{\ddot{X}\}_{i+1} \quad (36)$$

Δt denotes the time step which is chosen as 10^{-4} second.

Extracting $\{\ddot{X}\}_{i+1}$ from equation (35):

$$\{\ddot{X}\}_{i+1} = \frac{1}{b\Delta t^2}\left[\{X\}_{i+1} - \{X\}_i - \Delta t\{\dot{X}\}_i\right] - \left(\frac{1}{2a}\{X\}_i - 1\right)\{\ddot{X}\}_i \quad (37)$$

(37) and (38) gives:

$$[\bar{K}]\{X\}_{i+1} = \{\bar{F}\}_{i+1} \quad (38)$$

Where

$$\{\bar{F}\}_{i+1} = \{F\}_{i+1} + [M]\left(\frac{1}{b\Delta t^2}\{X\}_i + \frac{1}{b\Delta t}\{\dot{X}\}_i + \left(\left(\frac{1}{2b} - 1\right)\right)\{\ddot{X}\}_i\right) + [C]\left(\frac{1a}{b\Delta t}\{X\}_i + \left(\frac{a}{b} - 1\right)\{\dot{X}\}_i + \left(\frac{\Delta t}{2}\right)\left(\frac{b}{a} - 1\right)\{\ddot{X}\}_i\right) \quad (39)$$

So, the residue is computed as follows:

$$R = [\bar{K}]\{X\}_{i+1} + F_{nl} - \{\bar{F}\}_{i+1} \quad (40)$$

To ensure the convergence of the Newton Raphson method coupled with the implicit Newmark algorithm, R should be higher than ε (R> ε). ε is a small predefined value.

If this criterion is not verified, the residue R is defined at the k+1 iteration by a Taylor expansion:

$$R_{i+1}^{k+1} = R_{i+1}^k + \left.\frac{\partial R}{\partial q}\right|_{i+1}^k \Delta q \quad (41)$$

R_{i+1}^{k+1} must be zero, so Δq is defined as:

$$\Delta q = \left(\left.\frac{\partial R}{\partial q}\right|_{i+1}^k\right)^{-1}\left(-R_{i+1}^k\right) \quad (42)$$

$\{X\}_{i+1}$, $\{\dot{X}\}_{i+1}$ and $\{\ddot{X}\}_{i+1}$ are identified at the k+1 iteration when Δq was computed.

5-Results:

The presented results are obtained in two operating conditions: steady condition then the run up condition regime.

Using the Euler method, fig. 4 shows the measured speed evolution of the electrical motor. Two distinguished distinct regimes A and B are shown. (A) is a stationary regime while (B) is a non-

stationary one, specifically a run-up regime which is characterized by the input shaft speed increase as shown in Figure 4.

Fig. 5 displays the measured driving torque during the run-up regime.

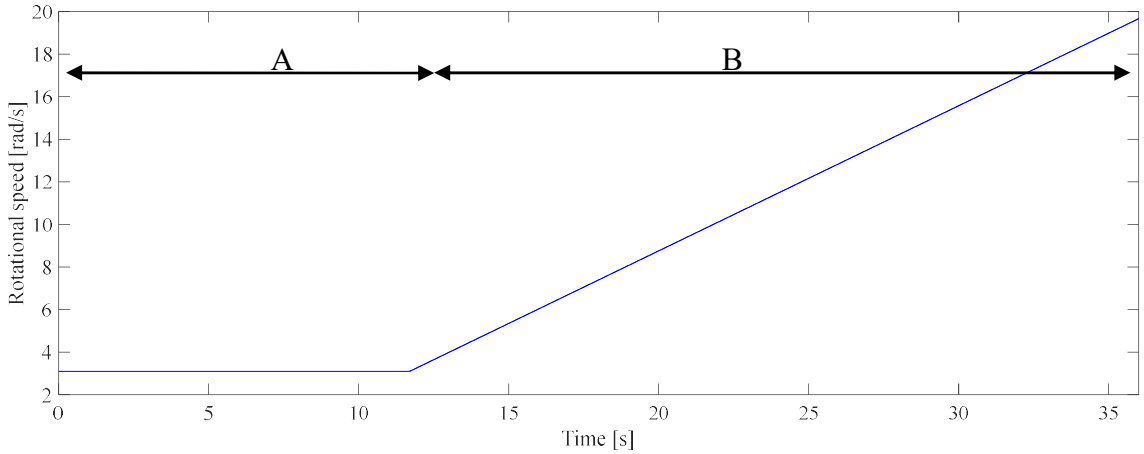

Fig. 4 Speed evolution of electrical motor

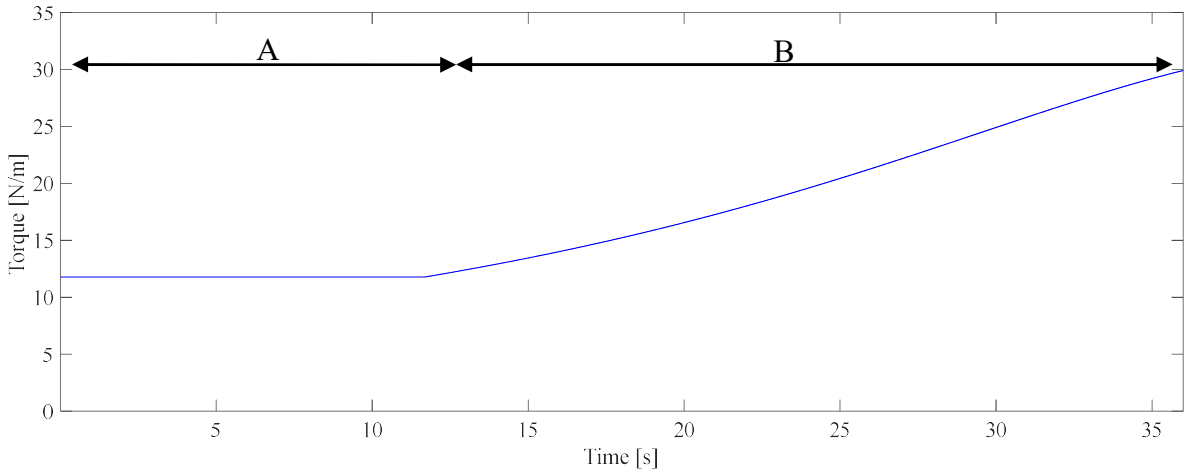

Fig. 5 Driven system mechanical characteristic

The input torque and the speed evolution presented in the two previous figures are induced in the numerical model in order to get the same running conditions.

Fig. 6 displays the acceleration on the fixed ring. The signal can be divided into two parts similarly to the evolution of the speed signal: part (B) presents run up régime, during this regime we can notice that the vibration is increasing. This phenomenon is due to the increasing of the accelerating torque.

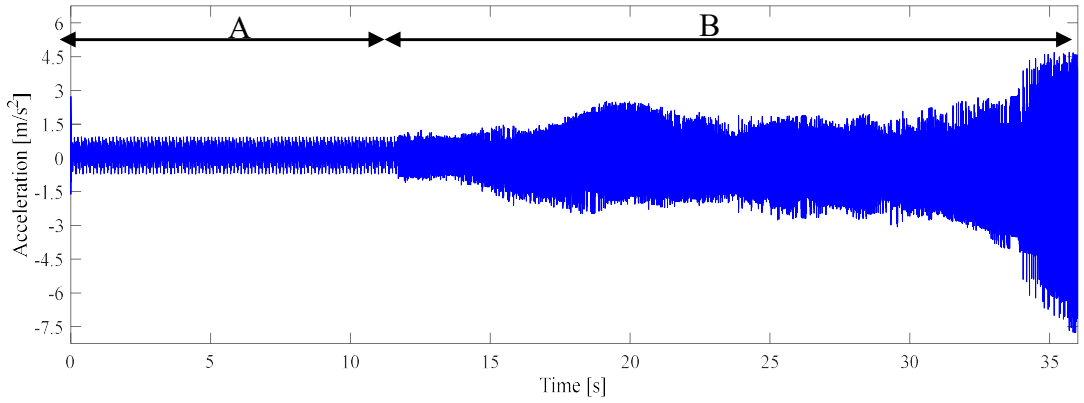

(a)

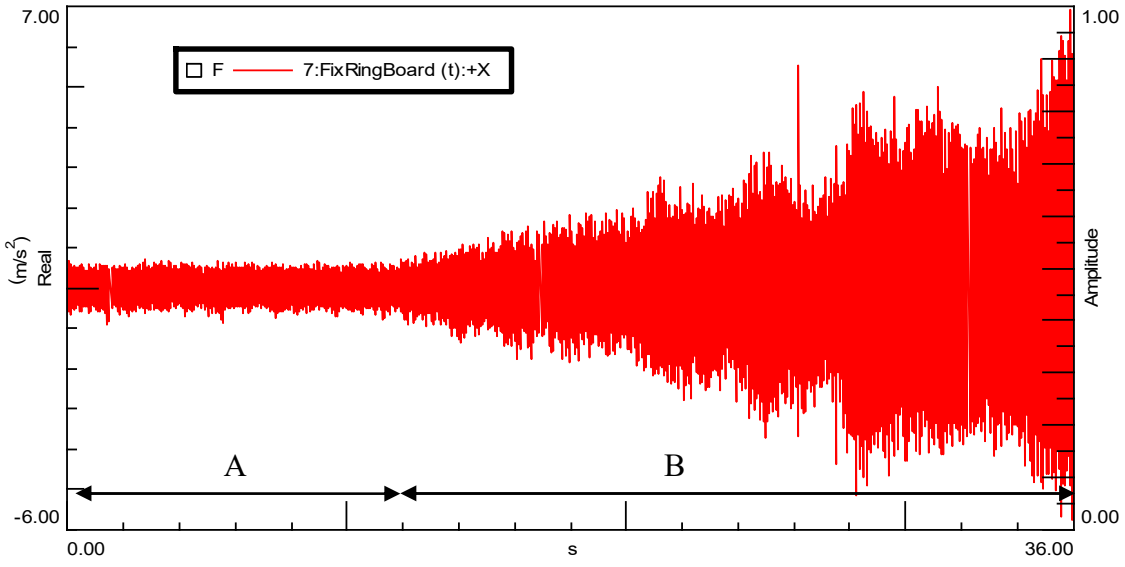

(b)

Fig. 6 Accelerations of the fixed ring (a) numerical result (b) experimental result

In part B while the speed is increasing (fig. 6), the acceleration signal time series have some amplitude modulations which are explained by crossing of the rotation frequency of motor with one of natural frequencies.

Fig. 7 shows the computed (HS) functions of the ring-planet1 and sun-planet1 respectively. The amplitude of HS is variable. The (HS) evolution is sensitive to the input torque applied to the planetary gear transmission. Thus, the mean value of this stiffness starts constant before acquiring its maximum in the run-up regime.

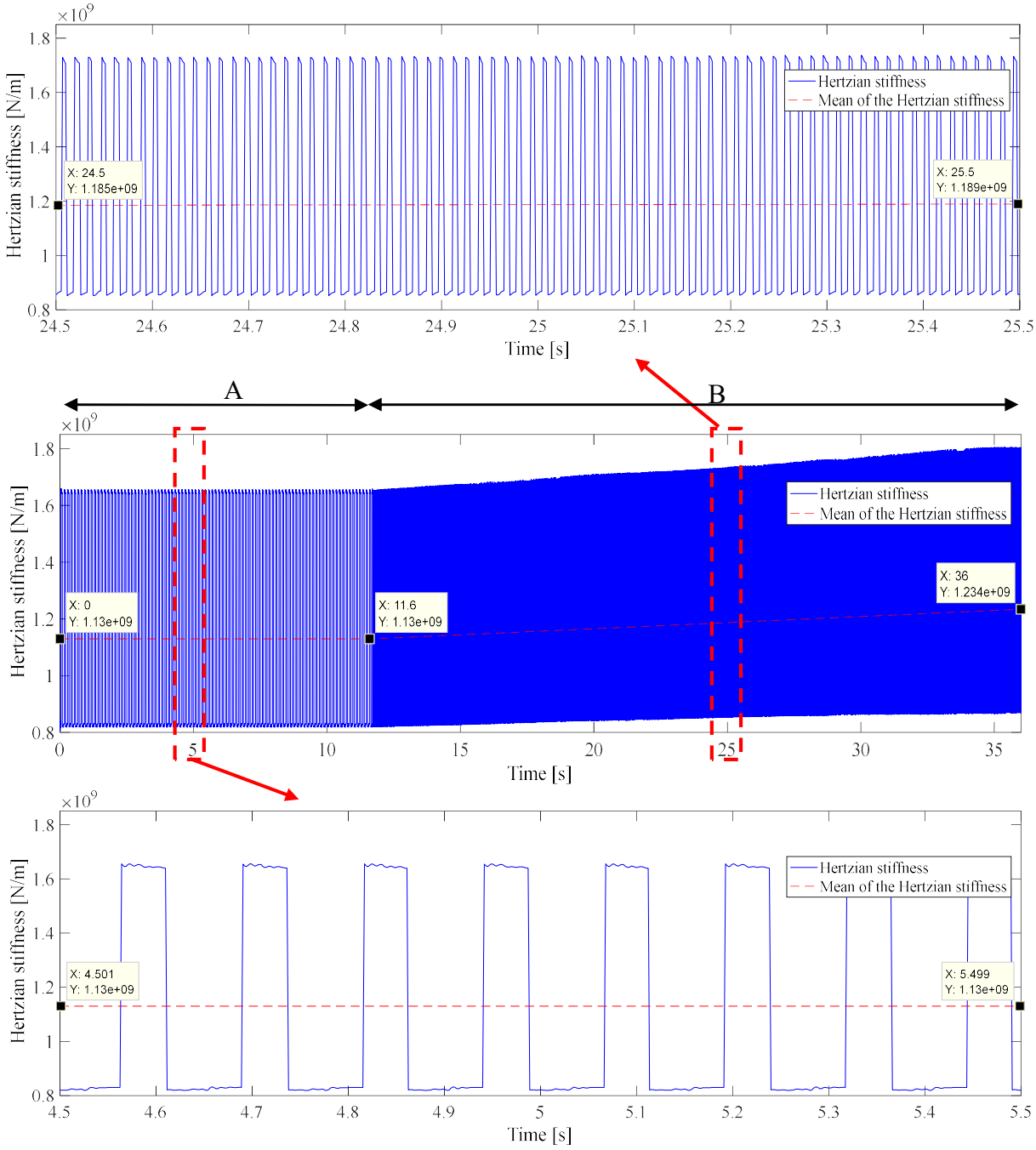
×10^9
Hertzian stiffness [N/m]
Time [s]
Hertzian stiffness
Mean of the Hertzian stiffness
X: 24.5
Y: 1.185e+09
X: 25.5
Y: 1.189e+09
A
B
X: 0
Y: 1.13e+09
X: 11.6
Y: 1.13e+09
X: 36
Y: 1.234e+09
X: 4.501
Y: 1.13e+09
X: 5.499
Y: 1.13e+09

(a)

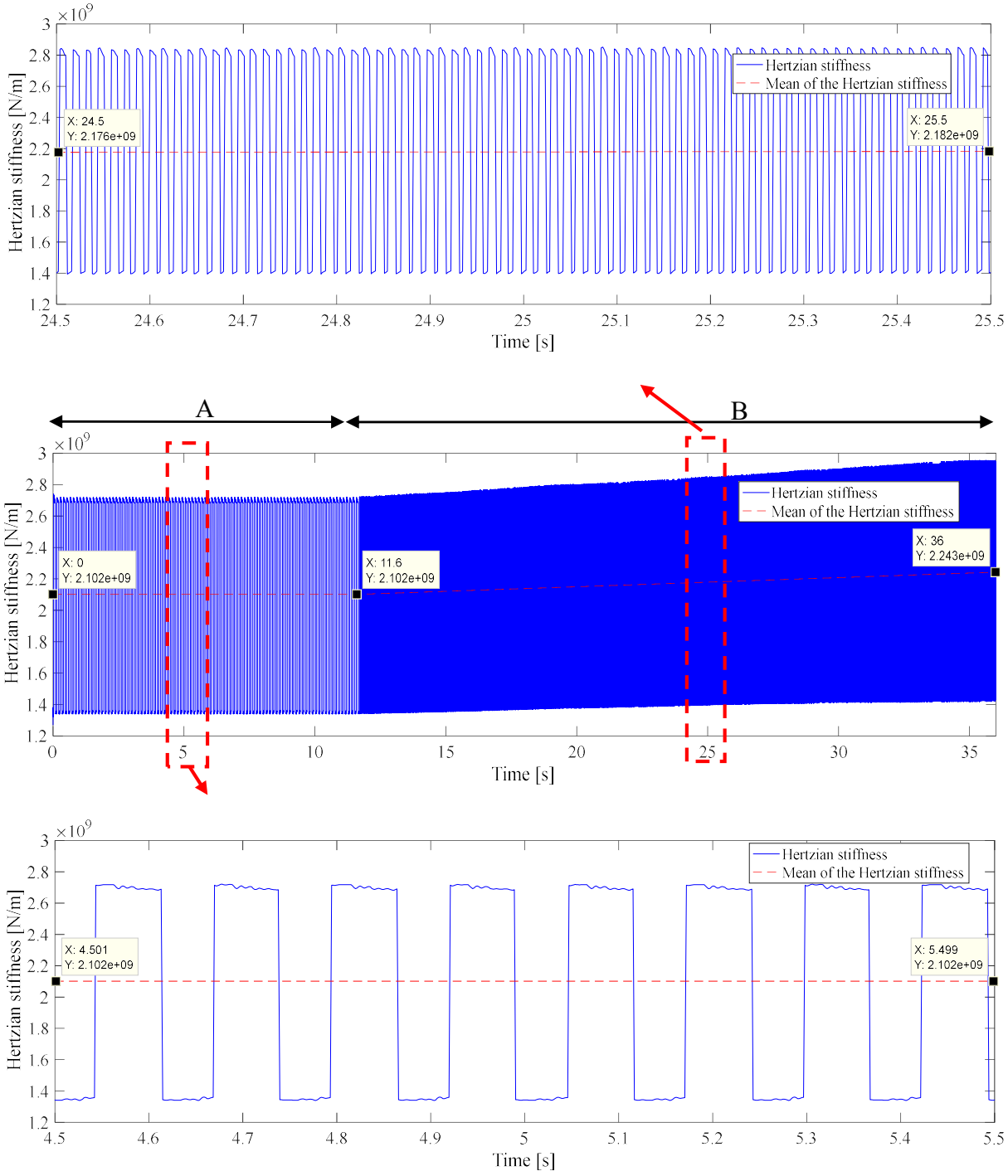

(b)

Fig. 7 (HS) evolution (a) sun-planet 1 (b) fixed ring-planet 1

According to equation (1), the (HS) of both sun-planets and planets-ring contacts is coupled to the (BS) and (FFS). Two (HS) behaviors of both sun-planets and planets-ring contacts are observed: in zone A, the mean and the period of fluctuation of (HS) is constant whereas the mean is increasing during run up (zone B) and the period of fluctuation is decreasing. In fact, the mean of (HS) of sun-planet 1 contact and ring-planet 1 contact are respectively increasing from 1.13×10^9 N.m to 1.234×10^9 N.m and from 2.102×10^9 N.m to 2.243×10^9 N.m.

This coupling allows computing of the gear mesh stiffness. Fig. 8 displays the gear mesh stiffness evolutions of sun-planet 1 and ring-planet 1 in which the mean evolutions are not the same in both regimes.

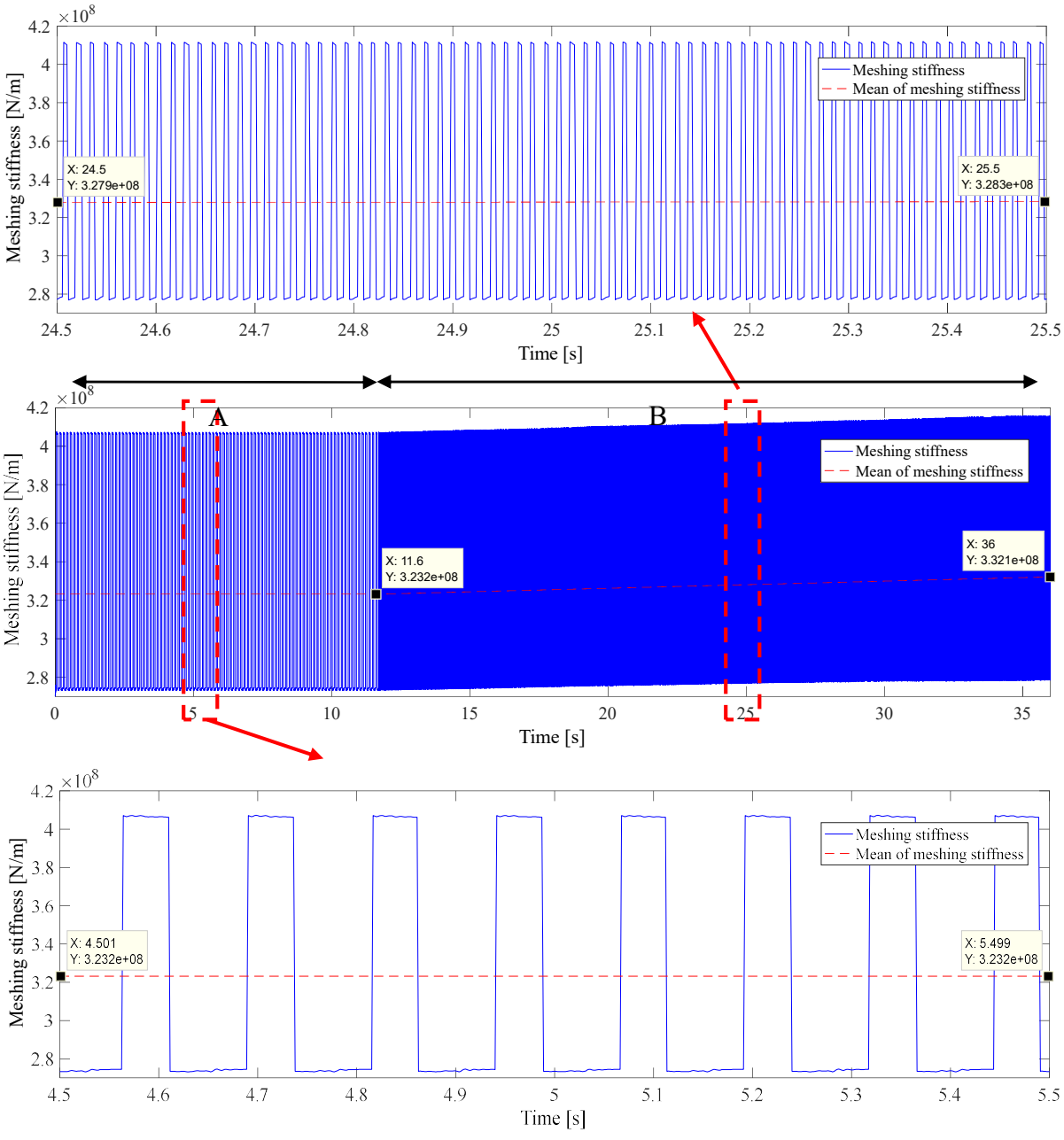

(a)

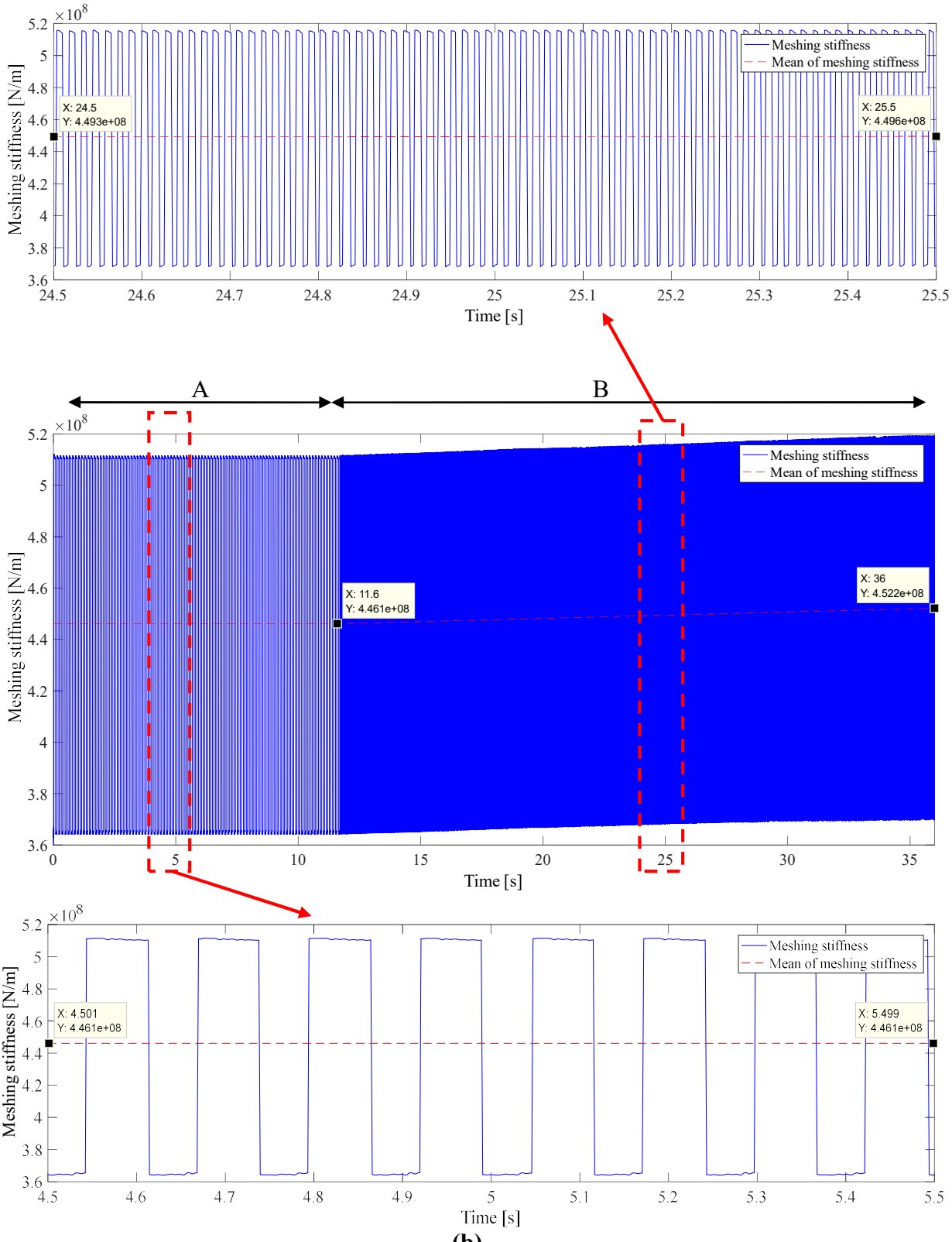

(b)

Fig. 8 Mesh stiffness evolution, (a) sun-planet 1 (b) fixed ring-planet 1

The gear mesh stiffness is steady in zone A in both sun-planets and planets-ring contacts whereas its mean values are increasing during run up.

To prove the influence of run-up regime on gear teeth, the (TE) and the inter mesh forces were carried out for all gear functions. The (TE) time evolution function matched to the ring-planet1 is presented in fig. 9. The (TE) attains a maximum value in the period (B). Nevertheless, they are constant during the first period (A).

The dynamic forces on teeth are computed according to the following equation:

$$F_d(t) = K_e(t)\delta(t) \tag{38}$$

Fig. 10 shows the meshing force between the ring and planet1. An overload behavior on teeth is observed during the run-up regime and it can cause defects [52].

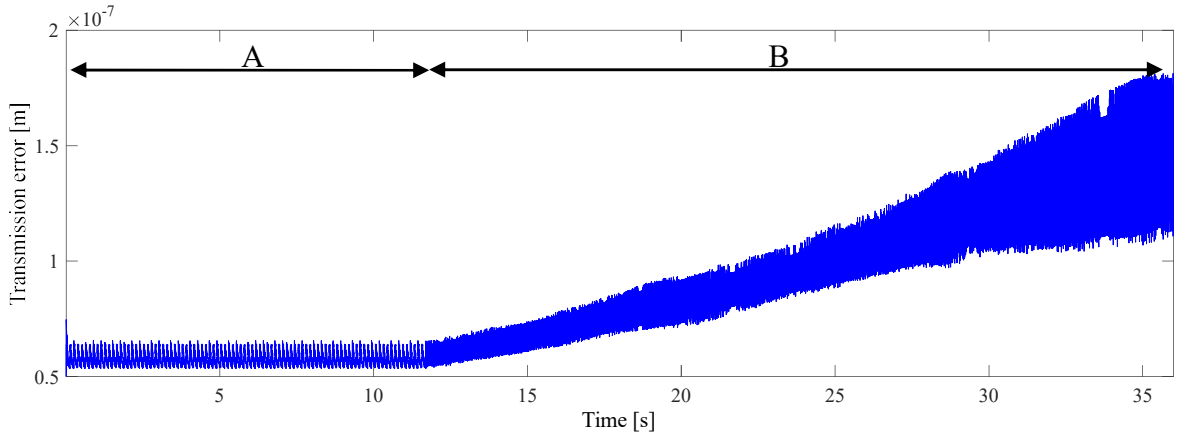

Fig. 9 (TE) function between the fixed ring and planets 1

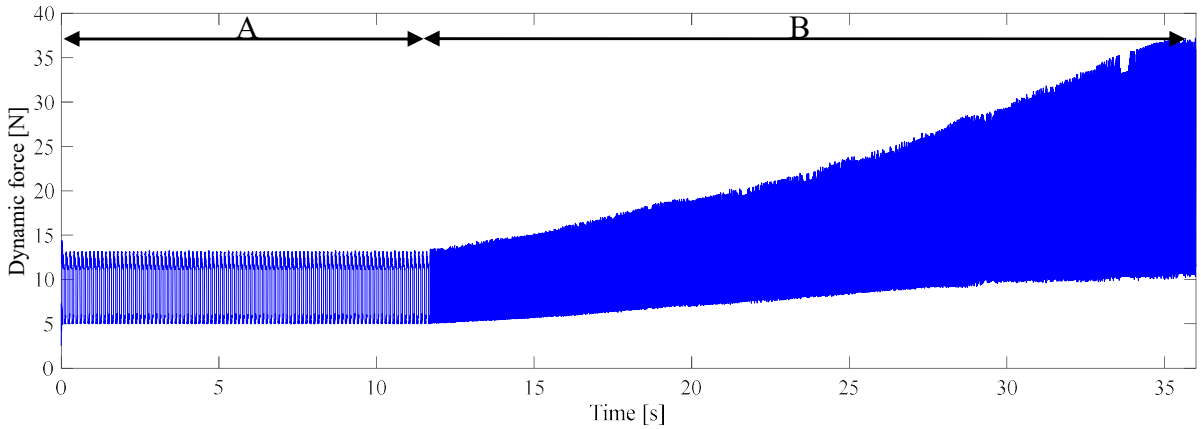

Fig. 10 Fixed ring-planet 1 meshing force

Fig. 11 displays a time-frequency map of the test ring acceleration with numerical simulation and experimental test. The two obtained behavior in time responses are also presented in both numerical and experimental results. From this figure, two different behaviors corresponding to the two parts A and B are shown. In part A, vertical lines appear, these lines show the stationary

regime, during which the speed is constant. In part B, the sloping lines show the mesh frequency with its harmonics increasing.

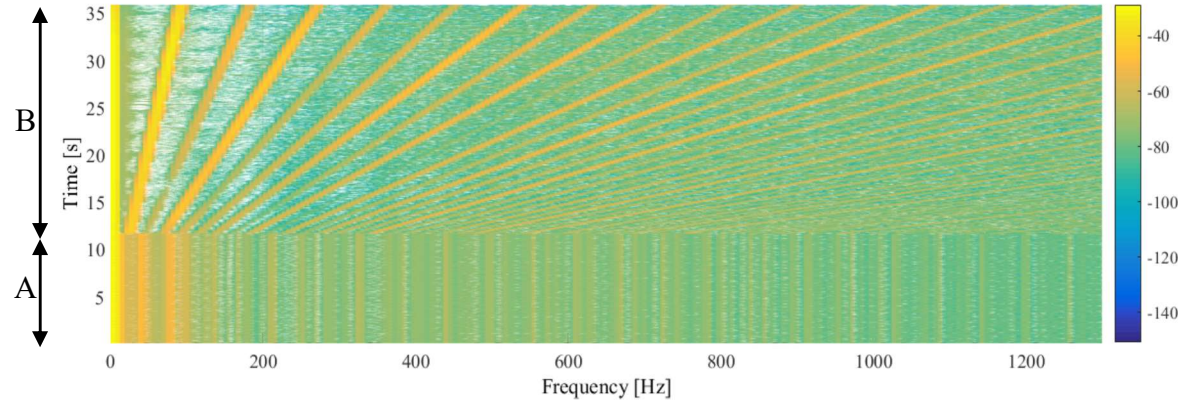

(a)

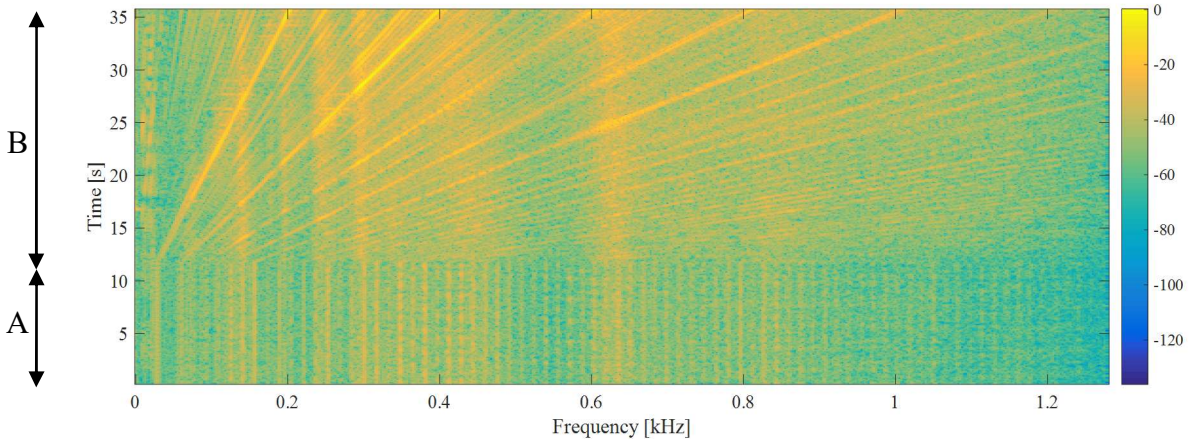

(b)

Fig. 11 STFT of acceleration of the fixed ring (a) numerical result (b) experimental result

6-Conclusion:

This paper examined the non-linear dynamic behavior of a back-to-back planetary gearbox transmission during stationary condition and then the run up regime. The objective was to characterize the dynamic behavior for such regimes when Hertzian contact between mating teeth is considered. To compute the mesh stiffness function which is the main excitation source of the transmission, bending, fillet foundation and Hertzian stiffness are put in parallel.

A torsional model combining the nonlinear mesh stiffness functions modeled in the different mesh zones and the non-stationary regime has been developed. The system's equation of motion is computed by using Newmark-β algorithm combined with Newton-Raphson technique. An experimental setup was used to validate numerical results. The main obtained results are listed as follows:

In the stationary condition, the mean of the Hertzian stiffness and the gear mesh stiffness are constant and the vibration level is steady. For the run-up regime, the mean value of the Hertzian stiffness and the gear mesh stiffness is increasing and the period of fluctuation is decreasing. The increasing acceleration torque and the variable gear mesh stiffness cause higher vibration levels, especially when the rotation frequency of motor cross with one of natural frequencies. The sensitivity inter-teeth dynamic force and transmission error to the run-up transient regime were also investigated showing an increase of the amplitude.

Seen the time varying frequency components, time frequency analysis was used to highlight the variation of gear mesh frequency and its harmonics during run-up regime. Experimental results confirmed the numerical ones. Future works will be dedicated to gear defect modeling and its influence on the nonlinear dynamic response of the planetary transmission.

Acknowledgements

This research work was supported by the Spanish Ministry responsible of Science and Technology through the project DPI2017-85390-P.

The authors gratefully thank the University of Cantabria cooperation project which supports the doctoral trainings of students of Sfax University.

The authors also acknowledge the Tunisian Project No. “19PEJC10-06”.

References:

1. Ognjanovi M, Risti M and Živkovi P, Reliability for design of planetary gear drive units, *Meccanica* 2014, 49: 829–841
2. Wang C and Cui HY, The analysis of power circulation and the simplified expression of the transmission efficiency of 2K-H closed epicyclic gear trains, *Meccanica* 2013, 48: 1071–1080
3. Wang S, Zhu C, Song C, Liu H, Tan J, Bai H, Effects of gear modifications on dynamic characteristics of wind turbine gearbox considering elastic support of the gearbox, *Journal of Mechanical Science and Technology* 2017, 31: 1079-1088
4. Zeng Z, Ding K, He G and Li W, Space-time model and spectrum mechanism on vibration signal for planetary gear drive, *Mechanical Systems and Signal Processing* 2019, 129: 164-185

5. Fatourehchi E, Mohammadpour M, King PD, Rahnejat H, Trimmer G, Williams A and Womersley R, Effect of mesh phasing on the transmission efficiency and dynamic performance of wheel hub planetary gear sets, *Proc IMechE, Part C: J Mechanical Engineering Science* 2017, 232: 3469-3481
6. Chen R, Zhou J and Sun W, Dynamic characteristics of planetary gear system based on contact status of the tooth surface, *Journal of Mechanical Science and Technology* 2018, 32: 1: 69-80
7. Hu Y, Ryali L, Talbot D and Kahraman A, A theoretical study of the overall transmission error in planetary gear sets, *Proc IMechE, Part C: J Mechanical Engineering Science* 2019, 233: 7200-7211
8. Dhouib S, Hbaieb R, Chaari F, Abbes MS, Fakhfakh T and Haddar M, Free vibration characteristics of compound planetary gear train sets, *Proc IMechE, Part C: J Mechanical Engineering Science* 2008, 222: 1389- 1401
9. Zhai H, Zhu C, Song C, Liu H, Li G, Ma F, Dynamic modeling and analysis for transmission system of high-power wind turbine gearbox, *Journal of Mechanical Science and Technology* 2015, 9: 10: 4073-4082
10. Feki N, Karray M, Khabou MT, Chaari F and Haddar M, Frequency analysis of a two-stage planetary gearbox using two different methodologies, *Comptes Rendus Mécanique* 2017, 345: 832-843
11. Rezaei M, Poursina M, Jazi SH, Aboutalebi FH, Calculation of time dependent mesh stiffness of helical planetary gear system using analytical approach, *Journal of Mechanical Science and Technology* 2018, 32:8:3537-3545
12. Daneshi-Far Z, Capolino GA, Henao H, Modeling and Simulation of Planetary Gearbox Effects on a Wound Rotor Induction Machine, *IEEE International Symposium on Industrial Electronics* 2012, 1234-1239
13. Y. Xing, T. Moan, Multi-body modelling and analysis of a planet carrier in a wind turbine gearbox, *Wind Energy* 2013, 16: 1067–1089
14. Chen X, Cheng G, Li H and Li Y, Fault identification method of planetary gear based on DT-CWT threshold denoising and LE, *Journal of Mechanical Science and Technology* 2017, 31:3:1035-1047
15. Thoret-Bauchet Q, Velex P, Guing M and and Casanova P, Simulations of the dynamic response of planetary gears in the presence of localised tooth faults, *Proc IMechE, Part C: J Mechanical Engineering Science* 2019, 233: 7212-7223

16. Lyu X, Hu Z, Zhou H, Wang Q, Application of improved MCKD method based on QGA in planetary gear compound fault diagnosis, *Measurement* 2019, 139:236-248
17. Moshrefzadeh A and Fasana A, Planetary gearbox with localised bearings and gears faults: simulation and time/frequency analysis, *Meccanica* 2017, 52:3759–3779
18. Jablonski A, Dworakowski Z, Dziedziech K, Chaari F, Vibration-based diagnostics of epicyclic gearboxes – From classical to soft-computing methods, *Measurement* 2019 147: 106811
19. Drago RJ, The Effect of Start-Up Load Conditions on Gearbox Performance and Life Failure Analysis, with Supporting Case Study, *American Gear Manufacturers Association Fall Technical Meeting* 2009, Michigan
20. Chaari F, Abbes MS, Viadero Rueda F, Fernandez del Rincon A, Haddar M, Analysis of planetary gear transmission in non-stationary operations, *Frontiers Mechanical Engineering* 2013 8: 88–94
21. Zimoroz R, Millioz F, Martin N, A procedure of vibration analysis from plan from planetary gearbox under non-stationary cyclic operations for instantaneous frequency estimation in time-frequency domain, *CM and MFPT* 2010, UK.
22. Vicuña CM and Chaari F, Analysis of a Planetary Gearbox Under Non-stationary Operating Conditions: Numerical and Experimental Results, *Advances in Condition Monitoring of Machinery in Non-Stationary Operations, Applied Condition Monitoring* 2016, 351-362
23. Lopatinskaia E, Zhu J, Mathew J, Monitoring varying speed machinery vibration- I. The use of non-stationary recursive filters, *Mechanical Systems and Signal Processing* 1995, 9: 635-645
24. Lopatinskaia E, Zhu J, Mathew J, Monitoring varying speed machinery vibration -II. Recursive filters and angle domain, *Mechanical Systems and Signal Processing* 1995 9:647-655
25. Meltzer G, Ivanov YY, Fault detection in gear drives with non-stationary rotational speed- part I: the time-frequency approach, *Mechanical Systems and Signal Processing* 2003, 17: 1033-1047
26. Meltzer G, Ivanov YY, Fault detection in gear drives with non-stationary rotational speed- part II: the time-quefrency approach, *Mechanical Systems and Signal Processing* 2003, 1: 273-283

27. Zimroz R, Urbanek J, Barszcz T, Bartelmus W, Millioz F, Martin N, Measurement of instantaneous shaft speed by advanced vibration signal processing- Application to wind turbine gearbox, *Metrology and measurement systems* 2011, 4: 701-712
28. Viadero F, Fernández A, Iglesias M, de-Juan A, Liaño E, Serna MA, Non-stationary dynamic analysis of a wind turbine power drive train: Offshore considerations, *Applied Acoustics* 2014 77: 204–211
29. Hammami A, Fernandez A, Chaari F, Viadero F and Haddar M, Dynamic behavior of back-to-back planetary gear in run up and run down transient regimes, *Journal of Mechanics* 2015, 31:4:481-491
30. Hammami A, Fernandez Del Rincon A, Viadero Rueda F, Chaari F, Haddar M, Back to Back Planetary gearbox: Influence of Non-stationary operating conditions, *International Gear Conference* 2014, 896-904.
31. Zhou S, Song G, Sun M and Ren Z, Nonlinear dynamic response analysis on gear-rotor-bearing transmission system, *Journal of Vibration and Control* 2016, 24:9:1632–1651
32. Chen S, Tang J, Chen W, Hu Z, Cao M, Nonlinear dynamic characteristic of a face gear drive with effect of modification, *Meccanica* 2014, 49:1023–1037
33. Fernandez A, Viadero F, Iglesias M, García P, De-Juan A, Sancibrian R, A model for the study of meshing stiffness in spur gear transmissions, *Mechanism and Machine Theory* 2013, 61:30–58
34. Guo Y, Keller J and Parker RG, Nonlinear dynamics and stability of wind turbine planetary gear sets under gravity effects, *European Journal of Mechanics-A/Solids* 2014, 47:45-57.
35. Zhao M and Ji JC, Nonlinear torsional vibrations of a wind turbine gearbox, *Applied Mathematical Modelling* 2015, 39:16:4928-4950.
36. Guo Y and Parker RG, Dynamic analysis of planetary gears with bearing clearance, *Journal of Computational and Nonlinear Dynamics* 2012, 7:4:041002.
37. Liu Z, Liu Z and Yu X, Dynamic modeling and response of a spur planetary gear system with journal bearings under gravity effects, *Journal of Vibration and Control* 2017, 24: 3569–3586
38. Bahk CJ and Parker RG, Analytical solution for the nonlinear dynamics of planetary gears, *Journal of Computational and Nonlinear Dynamics* 2011, 6:2:021007.
39. Parker RG, Agashe V and Vijayakar SM, Dynamic response of a planetary gear system using a finite element/contact mechanics model, *Journal of Mechanical Design* 2011, 122:3: 304-310.

40. Velex P and Flamand L, Dynamic response of planetary trains to mesh parametric excitations, *Journal of Mechanical Design* 1996, 118:1:7-14.
41. Xiang L, Gao N and Hu A, Dynamic analysis of a planetary gear system with multiple nonlinear parameters, *Journal of Computational and Applied Mathematics* 2018, 327: 325-340.
42. Ambarisha VK and Parker RG, Nonlinear dynamics of planetary gears using analytical and finite element models, *Journal of sound and vibration* 2007, 302:3:577-595.
43. Bouchaala N, Chaari F, Khabou MT, Fakhfakh T and Haddar M, Influence of the non-linear Hertzian stiffness on the dynamics of a spur gear system under transient regime and tooth defects, *International Journal of Vehicle Noise and Vibration* 2011, 7:2:149-177.
44. Hammami A, Fernandez A, Chaari F, Viadero F and Haddar M, Modal analysis of back-to-back planetary gear: experiments and correlation against lumped parameter model, *Journal of Theoretical and Applied Mechanics* 2015, 53:1:125–38
45. Mbarek A, Hammami A, Fernández A, Chaari F, Viadero F, Haddar M, Effect of load and meshing stiffness variation on modal properties of planetary gear, *Applied Acoustics* 2019, 147:32-43
46. Mbarek A, Fernández A, Hammami A, Iglesias M, Chaari F, Viadero F and Haddar M, Comparison of experimental and operational modal analysis on a back to back planetary gear, *Mechanism and Machine Theory* 2018, 124:226-247
47. Hammami A, Fernandez A, Chaari F, Iglesias M, Viadero F and Haddar M, Effects of variable loading conditions on the dynamic behaviour of planetary gear with power recirculation, *Measurement* 2016, 94:306–15
48. Cornell RW, Compliance and stress sensitivity of spur gear teeth, *Journal of Mechanical* Design 1981, 103:398–309.
49. Muskhelishvili NL, *Some Basic Problems of the Mathematical Theory of Elasticity*. 2nd edition P. Noor dhoff Limited 1975, The Netherlands.
50. Sainsot P, Velex P and Duverger O, Contribution of gear body to tooth deflections – a new bidimensional analytical formula, *Journal of Mechanical Design* 2004, 126:748–752.
51. Harsha SP, Nonlinear dynamic analysis of a high-speed rotor supported by rolling element bearings, *Journal of Sound and Vibration* 2006, 290:65–100.

52. Freese T and Hill C, Guidelines for preventing torsional vibration problems in Reciprocating machinery, In *Gas Machinery Conference* 2002, Nashville.